nature geoscience

LETTERS

PUBLISHED ONLINE: 12 SEPTEMBER 2016 | DOI: 10.1038/NGEO2796

Earthquake potential revealed by tidal influence on earthquake size–frequency statistics

Satoshi Ide[1]*, Suguru Yabe[1] and Yoshiyuki Tanaka[2]

The possibility that tidal stress can trigger earthquakes is long debated[1–6]. In particular, a clear causal relationship between small earthquakes and the phase of tidal stress is elusive[2–8]. However, tectonic tremors deep within subduction zones are highly sensitive to tidal stress levels[9–13], with tremor rate increasing at an exponential rate with rising tidal stress[11–13]. Thus, slow deformation and the possibility of earthquakes at subduction plate boundaries may be enhanced during periods of large tidal stress. Here we calculate the tidal stress history, and specifically the amplitude of tidal stress, on a fault plane in the two weeks before large earthquakes globally, based on data from the global[14], Japanese[15], and Californian[16] earthquake catalogues. We find that very large earthquakes, including the 2004 Sumatran, 2010 Maule earthquake in Chile and the 2011 Tohoku-Oki earthquake in Japan, tend to occur near the time of maximum tidal stress amplitude. This tendency is not obvious for small earthquakes. However, we also find that the fraction of large earthquakes increases (the *b*-value of the Gutenberg–Richter relation decreases) as the amplitude of tidal shear stress increases. The relationship is also reasonable, considering the well-known relationship between stress and the *b*-value[17–20]. This suggests that the probability of a tiny rock failure expanding to a gigantic rupture increases with increasing tidal stress levels. We conclude that large earthquakes are more probable during periods of high tidal stress.

Tidal deformations of the Earth due to motions of the Sun and Moon cause changes in the stress state, which may trigger earthquakes. The possibility of tidal triggering of earthquakes has been investigated since the 19th century[1], and numerous studies have examined this topic[2–8]. Statistically significant correlations between seismicity and tidal stress have been discovered using large data sets, but the correlations are generally limited to special regions or circumstances. For example, seismicity was correlated with tidal stress changes before three large earthquakes in Sumatra[7] and before the 2011 Tohoku-Oki earthquake in Japan[8]. While such observations are of interest in the field of probabilistic earthquake forecasting, the governing mechanism that underlies the correlations is unknown. In more general cases, tidal stress changes on the order of several kPa are considered too small to control the dynamic rupture processes of earthquakes, which are characterized by stress changes on the order of MPa.

The recent discovery of deep tectonic tremors in plate boundary regions has slightly modified our view of the relationship between tidal stresses and earthquakes, as these tremors are sometimes highly sensitive to tidal stress changes[9–13], with tremor rates showing an exponential increase in proportion to the applied encouraging stress[11–13]. Thus, even stress changes of only a few kPa can amplify the tremor rate by several orders. As tremors reflect slow slip on the plate interface, tidal stresses also accelerate the slow slip on the plate interface. The slow slip may not be restricted in deep plate boundary regions, rather it can be ubiquitous in seismic regions. Therefore, such accelerated slow deformation can change the stress state on the entire seismic region, and hence increase the probability of earthquakes.

While such slow deformation is dependent on the amplitude of the tidal stress, most previous studies on this topic have investigated only the phase of the tidal stress rather than its amplitude. The amplitude of the tidal stress increases at times of syzygies (new moon or full moon) and spring tides in the ocean, which occur at periodicities of 14.8 days. Several studies have investigated the relationship between syzygies and earthquakes. Kennedy *et al.* noted that large (>M7.0) earthquakes appear to occur more frequently near times of syzygies, but they could not confirm the relationship statistically[5]. In fact, the relationship tends to weaken and disappear as smaller events are considered.

To investigate the possible effects of the tidal stress amplitude on earthquake occurrence, we calculated temporal changes in tidal stress components on a known earthquake fault plane, as described in the Methods[21–25]. Figure 1 shows tidal shear stresses before and after the three most recent large earthquakes. The 2004 Sumatra and 2010 Maule earthquakes both occurred near the time of a full moon, close to the peak of the tidal shear stress. The 2011 Tohoku-Oki earthquake, on the other hand, occurred near the time of a neap tide (Fig. 1b). Nevertheless, the tidal shear stress showed consistently large amplitude around the time of the Tohoku-Oki earthquake. Many very large earthquakes have occurred close to the time of large shear stresses caused by syzygies, as shown in Supplementary Fig. 1. However, the correlation between the tidal shear stress and earthquake occurrence is not always clear, as at least three events (15/11/2006, 13/01/2007, and 12/09/2007) in Supplementary Fig. 1 did not correlate with large tidal stress, and a deterministic relationship has not been demonstrated.

Because the amplitude variations of the tidal stress are not always regular (Fig. 1 and Supplementary Fig. 1), a simple phase analysis that assumes a constant period may not be effective in examining the effect of tidal stress on seismicity. Therefore, as an alternative, the relationship between the maximum tidal shear stress during the one day preceding an earthquake (the coseismic maximum) and the daily maxima during the 15 days before the event (the preseismic period) were examined, and the ranking (1 for the lowest, 15 for the highest) of the coseismic maximum was recorded (Supplementary Fig. 2). The coseismic maximum rankings for the Sumatra, Tohoku-Oki, and Maule earthquakes are 11, 13, and 15, respectively.

The choice of a one-day period was based on the assumption that slow deformation due to tidal stresses has a certain duration, and also because some preparation processes might occur before an earthquake. The assumption of a one-day period is convenient for

[1]Department of Earth and Planetary Science, University of Tokyo, 7-3-1 Hongo, Bunkyo, Tokyo 113-0033, Japan. [2]Earthquake Research Institute, University of Tokyo, 1-1-1 Yayoi, Bunkyo, Tokyo 113-0032, Japan. *e-mail: ide@eps.s.u-tokyo.ac.jp

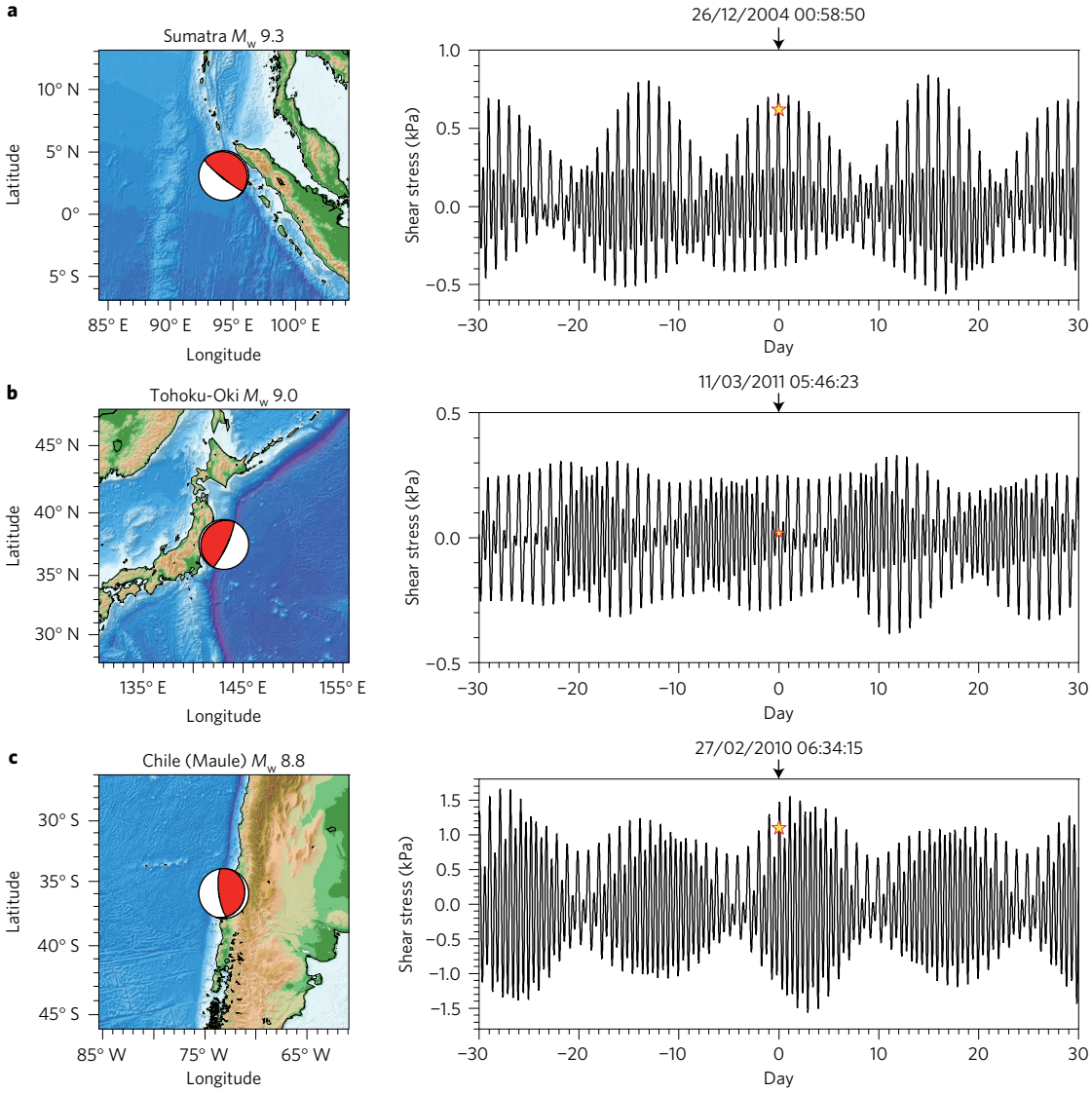

Figure 1 | Tidal shear stress for the period 30 days before and after three large earthquakes. a, The 2004 Sumatra earthquake. **b**, The 2011 Tohoku-Oki earthquake. **c**, The 2010 Chile Maule earthquake. Left: location maps and focal mechanism. Right: shear stress changes resolved on the fault plane in the direction of slip. Stars represent the timing of the earthquakes and the stress levels at that time.

also capturing the potential effects of the normal stress[4], which is often correlated (positively or negatively) with the shear stress, and the timing of both the positive and negative peaks of the normal and Coulomb stresses typically falls within the one-day period. Nevertheless, since the period measuring the coseismic maximum (coseismic period) is arbitrary, we also test two cases, by recording the ranking of the coseismic maximum in half day or two days in 15 or 14 days of the preseismic period, respectively.

The calculations of rankings were made for all events in the Global Central Moment Tensor (CMT) catalogue[14] exceeding M_w 5.5. Figure 2 shows histograms of rankings for shallow (depth < 100 km) events in the Global CMT catalogue, with different thresholds for the minimum magnitude. Figure 2a,b shows the dominance of large rankings (75% or 40% in the five large rankings) for the largest 12 and 123 events, respectively. The differences between bins diminish as the number of events increases, and the difference is small for earthquakes exceeding M_w 5.5 (>10,000 events) (Fig. 2d). The distribution in Fig. 2d is indistinguishable from the distribution made by random sampling of event timing. Thus, if only the frequency of medium and large earthquakes is examined, a correlation between earthquake occurrence and the amplitude of the tidal stress would be rejected, as concluded by Kennedy and colleagues[5].

A more complex but better fitting interpretation of the data in Fig. 2, however, is that for more than 10,000 events of $\sim M_w$ 5.5 in the catalogue, an event that occurred under a large tidal stress had a greater likelihood of growing to an $M_w > 8$ event. Such an interpretation would indicate that the slope of the power-law size–frequency statistic (that is, the b-value of the Gutenberg–Richter relationship) is different for each ranking of the tidal stress. Figure 3a shows size–frequency statistics and b-values (with standard deviations) estimated using the maximum likelihood method[26]. As expected from Fig. 2, the b-value decreases as the stress ranking increases. For the bottom five stress rankings, the b-value is 1.15, but the b-value decreases to 0.93 for the top five stress rankings. The difference is statistically significant, as confirmed by Utsu's test[27] (see Methods). Similar results are obtained for different coseismic periods (Supplementary Figs 3 and 4).

In the global catalogue, differences in b-values are less clear for events of $M_w < 6.5$, possibly because the catalogue includes events with various focal mechanisms in diverse tectonic environments, and hence mixes events with a wide range of b-values[17,18].

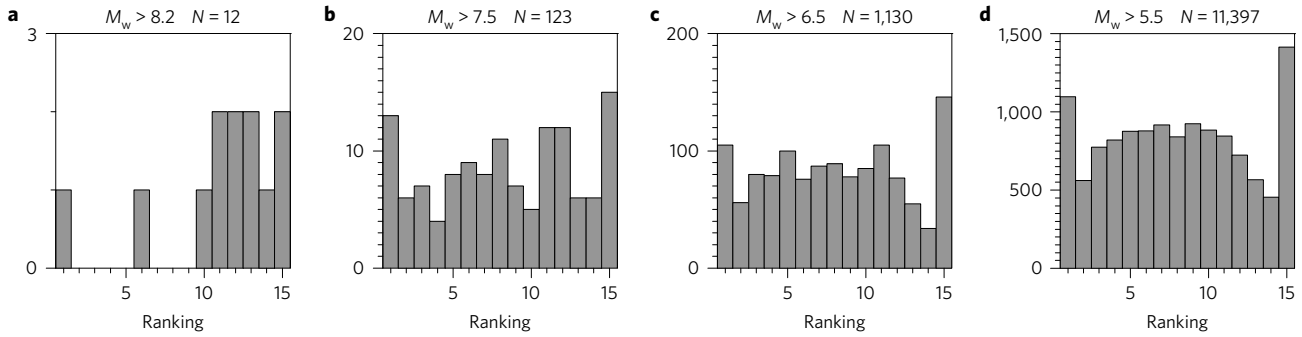

Figure 2 | Histograms of stress level ranking for different magnitude thresholds. a–d, Ranking of the maximum shear stress on the day of an earthquake, as compared with the daily maxima during the 15 days before the event, for earthquakes larger than magnitude thresholds of M_w 8.2 (**a**), M_w 7.5 (**b**), M_w 6.5 (**c**) and M_w 5.5 (**d**). Results are based on the Global CMT.

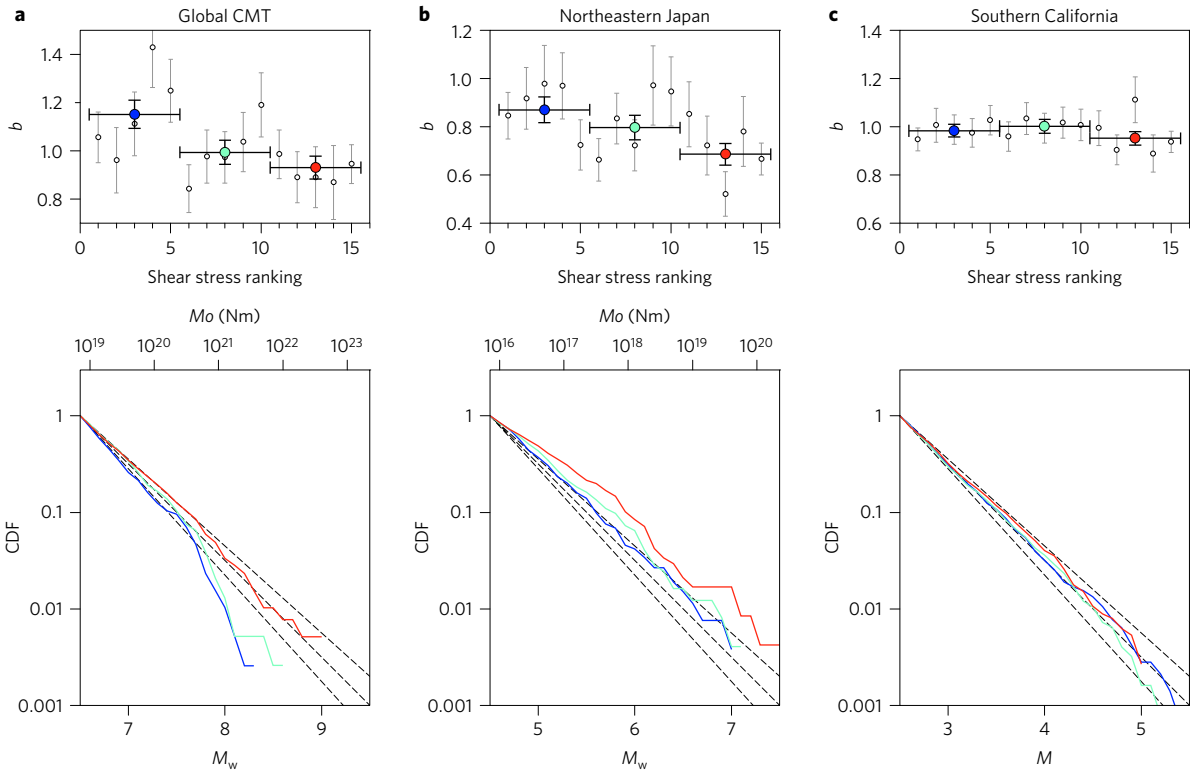

Figure 3 | Estimated *b*-values and size-frequency statistics. a, Global shallow earthquakes larger than M_w 6.5. **b**, Low-angle thrust-type earthquakes in northeastern Japan, larger than M_w 4.5. **c**, Strike-slip-type earthquakes in southern California, larger than M 2.5. Top: open circles show the *b*-values independently estimated for 15 stress rankings, showing the standard deviation for each stress ranking. Blue, light blue, and red circles show *b*-values calculated using 5 stress rankings, as indicated by the horizontal bar. Bottom: magnitude–frequency statistics. Each line represents the statistics for a shear stress level shown in the corresponding colour in the top panel. Three dashed lines show distributions corresponding to $b = 0.9$, 1.0, and 1.1.

To consider more homogeneous tectonic environments and less variable focal mechanisms, we also separately analysed earthquakes occurring in Japan and California (see Methods).

Figure 3b shows results using the F-net MT catalogue[15] for a relatively homogeneous region in northeastern Japan, including the Hokkaido and Tohoku regions. Only low-angle thrust-type earthquakes are considered because they have fairly uniform *b*-value, although similar results are obtained for all events. Since thrust-type earthquakes have a relatively small *b*-value[18], *b*-values are generally small. Moreover, the *b*-values decrease with increasing stress levels, and very small *b*-values (~0.7) are observed in cases of large tidal stress levels. Figure 3c presents another example of strike-slip-type earthquakes from 'The Refined Earthquake Focal Mechanism Catalog for Southern California'[16]. The *b*-values are generally large, with slightly smaller values for higher tidal stress levels, although the significance is weaker than other two cases. Similar results are obtained for longer coseismic periods (Supplementary Fig. 3), but the trend is relatively weak for half-day coseismic period (Supplementary Fig. 4), suggesting the importance of diurnal tides.

In northeastern Japan, the separation of size–frequency statistic curves is visible even for events of ~M_w 5 (Fig. 3b), indicating that tidal controls are apparent for smaller earthquakes in some environments. In Fig. 3b, among the 237 and 263 events of M_w 4.5, 116 and 98 grew into events larger than M_w 5, for higher (11–15) and lower (1–5) rankings, respectively. Assuming that the earthquake growth process between two sizes is governed by a binomial distribution with probability $p = 98/263$ for low stress rankings, the chance that we have 116 events over M_w 5 from 237 events of M_w 4.5 is smaller than 10^{-4}.

The correspondence of small *b*-values and earthquakes with large shear stresses is consistent with evidence from previous studies on acoustic emissions in rock experiments, showing decreasing *b*-values with increasing differential stresses[19,20], variations in *b*-values with the type of earthquake focal mechanism[18], and positive correlations between *b*-values and the ages of subducting plates worldwide[17]. Although the growth processes of dynamic rupture are not fully understood, one hypothesis is that growth occurs via a cascading process in a hierarchical system, from a tiny rock failure to a giant earthquake[28,29]. Rupture is accelerated and decelerated controlled by energy balance, and small changes of stress distribution may determine growth and arrest of rupture[29,30]. Based on this type of model, it is possible to interpret the observation that large tidal stresses correspond to a high probability of cascading rupture growth, which is the probability of an event progressing from small to large scales. Small tidal stress can enhance slow deformation in various scales, and resultant stress redistribution is likely to increase the cascading probability of nearly critical dynamic rupture.

Every day, numerous small earthquakes occur worldwide. A very small fraction of these events grows into giant earthquakes. It is a long-standing problem as to whether we can estimate the final size of an earthquake at the moment of initiation of a dynamic rupture from a small nucleus. The present results suggest that the final earthquake size can be estimated probabilistically. For example, for *b*-values of 1.1 and 0.9 (corresponding to periods of low and high stress, respectively), the probability that an M_w 5 event will grow to an M_w 9 event is increased by a factor of six under high-stress (low *b*-value) as compared to low-stress (high *b*-value) conditions. If the same mechanism operates starting from M_w 1 events, the increase in probability would be by a factor of ~40. Thus, knowledge of the tidal stress state in seismic regions can be used to improve probabilistic earthquake forecasting, especially for extremely large earthquakes.

Methods

Methods, including statements of data availability and any associated accession codes and references, are available in the online version of this paper.

Received 6 April 2016; accepted 22 July 2016;
published online 12 September 2016

References

1. Schuster, A. On lunar and solar periodicities of earthquakes. *Proc. R. Soc. Lond.* **61,** 455–465 (1897).
2. Tsuruoka, H., Ohtake, M. & Sato, H. Statistical test of the tidal triggering of earthquakes: contribution of the ocean tide loading effect. *Geophys. J. Int.* **122,** 183–194 (1995).
3. Vidale, J. E., Agnew, D. C., Johnston, M. J. S. & Oppenheimer, D. H. Absence of earthquake correlation with Earth tides: an indication of high preseismic fault stress rate. *J. Geophys. Res.* **103,** 24567–24572 (1998).
4. Cochran, E. S., Vidale, J. E. & Tanaka, S. Earth tides can trigger shallow thrust fault earthquakes. *Science* **306,** 1164–1166 (2004).
5. Kennedy, M., Vidale, J. E. & Parker, M. G. Earthquakes and the moon: syzygy predictions fail the test. *Seismol. Res. Lett.* **75,** 607–612 (2004).
6. Métivier, L. *et al*. Evidence of earthquake triggering by the solid earth tides. *Earth Planet. Sci. Lett.* **278,** 370–375 (2009).
7. Tanaka, S. Tidal triggering of earthquakes precursory to the recent Sumatra megathrust earthquakes of 26 December 2004 (Mw 9.0), 28 March 2005 (Mw 8.6), and 12 September 2007 (Mw 8.5). *Geophys. Res. Lett.* **37,** L02301 (2010).
8. Tanaka, S. Tidal triggering of earthquakes prior to the 2011 Tohoku-Oki earthquake (Mw 9.1). *Geophys. Res. Lett.* **39,** L00G26 (2012).
9. Rubinstein, J. L., La Rocca, M., Vidale, J. E., Creager, K. C. & Wech, A. G. Tidal modulation of nonvolcanic tremor. *Science* **319,** 186–189 (2008).
10. Nakata, R., Suda, N. & Tsuruoka, H. Non-volcanic tremor resulting from the combined effect of Earth tides and slow slip events. *Nat. Geosci.* **1,** 676–678 (2008).
11. Thomas, A. M., Bürgmann, R., Shelly, D. R., Beeler, N. M. & Rudolph, M. L. Tidal triggering of low frequency earthquakes near Parkfield, California: implications for fault mechanics within the brittle–ductile transition. *J. Geophys. Res.* **117,** B05301 (2012).
12. Ide, S. & Tanaka, Y. Controls on plate motion by oscillating tidal stress: evidence from deep tremors in western Japan. *Geophys. Res. Lett.* **41,** 3842–3850 (2014).
13. Houston, H. Low friction and fault weakening revealed by rising sensitivity of tremor to tidal stress. *Nat. Geosci.* **8,** 409–415 (2015).
14. Ekström, G., Nettles, M. & Dziewonski, A. M. The global CMT project 2004–2010 centroid-moment tensors for 13,017 earthquakes. *Phys. Earth Planet. Inter.* **200–201,** 1–9 (2012).
15. Fukuyama, E., Ishida, M., Dreger, D. S. & Kawai, H. Automated seismic moment tensor determination by using on-line broadband seismic waveforms. *Zisin* **51,** 149–156 (1998).
16. Yang, W., Hauksson, E. & Shearer, P. M. Computing a large refined catalog of focal mechanisms for southern California (1981–2010): temporal stability of the style of faulting. *Bull. Seismol. Soc. Am.* **102,** 1179–1194 (2012).
17. Nishikawa, T. & Ide, S. Earthquake size distribution in subduction zones linked to slab buoyancy. *Nat. Geosci.* **7,** 904–908 (2014).
18. Schorlemmer, D., Wiemer, S. & Wyss, M. Variations in earthquake-size distribution across different stress regimes. *Nature* **437,** 539–542 (2005).
19. Scholz, C. H. The frequency-magnitude relation of microfracturing in rock and its relation to earthquakes. *Bull. Seismol. Soc. Am.* **58,** 399–415 (1968).
20. Goebel, T. H. W., Schorlemmer, D., Becker, T. W., Dresen, G. & Sammis, C. G. Acoustic emissions document stress changes over many seismic cycles in stick-slip experiments. *Geophys. Res. Lett.* **40,** 2049–2054 (2013).
21. Okubo, S. & Tsuji, D. Complex Green's function for diurnal/semidiurnal loading problems. *J. Geod. Soc. Jpn* **47,** 225–230 (2001).
22. Agnew, D. C. *SPOTL: Some Programs for Ocean-Tide Loading* SIO Technical Report (Scripps Institution of Oceanography, 2012).
23. Egbert, G. D. & Erofeeva, S. Y. Efficient inverse modeling of barotropic ocean tides. *J. Atmos. Ocean. Technol.* **19,** 183–204 (2002).
24. Matsumoto, K., Takanezawa, T. & Ooe, M. Ocean tide models developed by assimilating TOPEX/POSEIDON altimeter data into hydrodynamical model: a global model and a regional model around Japan. *J. Oceanogr.* **56,** 567–581 (2000).
25. Yabe, S., Tanaka, Y., Houston, H. & Ide, S. Tidal sensitivity of tectonic tremors in Nankai and Cascadia subduction zones. *J. Geophys. Res.* **120,** 7587–7605 (2015).
26. Aki, K. Maximum likelihood estimate of b in the formula $\log N = a - bM$ and its confidence limits. *Bull. Earthq. Res. Inst.* **43,** 237–239 (1965).
27. Utsu, T. Representation and analysis of the earthquake size distribution: a historical review and some new approaches. *Pure Appl. Geophys.* **155,** 509–535 (1999).
28. Fukao, Y. & Furumoto, M. Hierarchy in earthquake size distribution. *Phys. Earth Planet. Inter.* **37,** 149–168 (1985).
29. Ide, S. & Aochi, H. Earthquakes as multiscale dynamic ruptures with heterogeneous fracture surface energy. *J. Geophys. Res.* **110,** B11303 (2005).
30. Madariaga, R. Criticality of rupture dynamics in 3-D. *Pure. Appl. Geophys.* **157,** 1981–2001 (2000).

Acknowledgements

We are grateful for helpful comments from H. Kao and J. Vidale. This work was supported by the Earthquake and Volcano Hazards Observation and Research Program, MEXT and JSPS KAKENHI (16H02219). Figures were prepared using the Generic Mapping Tools (Wessel and Smith, 1998).

Author contributions

S.I. designed the plan of study, carried out tidal stress calculations and the statistical analysis, and wrote the manuscript. S.Y. and Y.T. developed a calculation system for the tidal stress and contributed to the discussion.

Additional information

Supplementary information is available in the online version of the paper. Reprints and permissions information is available online at www.nature.com/reprints. Correspondence and requests for materials should be addressed to S.I.

Competing financial interests

The authors declare no competing financial interests.

Methods

Earthquake catalogue. Three catalogues were used for location and mechanism information: the Global Central Moment Tensor (CMT) catalogue[14] for global earthquakes of $M_w > 5.5$, from 1976 to 2015; the NIED F-net moment tensor (MT) catalogue[15] for earthquakes in northeastern Japan of $M_w > 4.5$, from 1997 to 2015; and 'The Refined Earthquake Focal Mechanism Catalog for Southern California'[16] for earthquakes in southern California of $M > 2.5$. Magnitude scales are moment magnitudes in the former two catalogues and local magnitudes in the California catalogue.

In Japan, the exact study area is a rectangular region, 35°–44° N latitude and 140°–146° E longitude. To study low-angle thrust events consistent with regional plate motions, we extracted events whose lower-angle plane was striking at 180°–270° and dipping at 5°–35°. Although the 2011 Tohoku-Oki earthquake and a number of its aftershocks are dominant in this catalogue, the completeness of the catalogue during the aftershock period is less sufficient, which may affect the *b*-value estimation. Therefore, all events occurring in March 2011 were removed in the generation of Fig. 3 (we also confirmed that inclusion of these events did not significantly alter the result).

In southern California, the exact study area is a rectangular region, 32°–36° N latitude and 120°–115° W longitude. We extracted events whose two nodal planes were nearly vertical (>75°). The catalogue is dominated by the aftershocks of the 1992 Landers earthquake, for which the completeness of the catalogue is uncertain. Therefore, we used events since 1993.

Calculation of tidal stress. The tidal stresses from the solid earth tide and ocean tide were calculated following Tsuruoka and colleagues[2]. The solid earth tides were calculated using the second and third terms of the Legendre polynomial expansion of the gravitational potential change due to the Sun and Moon. The ocean tides were calculated as the elastic response of the ocean mass change. Green's functions were used for both calculations, prepared using the code of Okubo and Tsuji[21], and assuming a PREM structure. The SPOTL code[22] was used to compute ocean loading with the ocean tide model of TPXO7.2ATLAS[23] for the Global CMT and California catalogues, and NAO99b[24] for the F-net MT catalogue. More details of the computation are explained in the appendix of Yabe and colleagues[25].

We calculated the shear stress on the fault plane of each earthquake. Each moment tensor solution has two nodal planes; the amplitudes of the shear stress acting on these two planes are common, while those of the normal stress differ. Therefore, we consider only the shear stress in the present study. Supplementary Fig. 1 shows more examples of the calculated tidal shear stress for large earthquakes.

Estimation of *b*-values and Utsu's test. The *b*-value is the slope of the power-law size–frequency distribution of earthquakes, calculated using a maximum likelihood estimation (MLE) method[26]. For N earthquakes with magnitudes $M_1, \ldots, M_N$, the MLE of b is given as

$$b^{\mathrm{MLE}} = \frac{\log_{10} e}{\sum M_i/N - M_c}$$

where M_c is the lower limit of the magnitude, above which the catalogue is complete. The standard deviation of b^{MLE} is calculated as

$$\sigma^{MLE} = b^{\mathrm{MLE}}/\sqrt{N}$$

When two groups of earthquakes are used to estimate *b*-values, the significance of the difference between the two groups can be measured using Utsu's test[27], in which Akaike's information criterion (AIC), ΔAIC, is computed as

$$\begin{aligned}\Delta\mathrm{AIC} \;=\; & -2(N_1+N_2)\ln(N_1+N_2) \\ & +2N_1\ln\left(N_1+\frac{N_2 b_1}{b_2}\right)+2N_2\ln\left(N_2+\frac{N_1 b_2}{b_1}\right)-2\end{aligned}$$

where N_1 and N_2 are the number of events, and b_1 and b_2 are the estimated *b*-values for the two groups. If ΔAIC exceeds 2, the difference is considered significant, and if it exceeds 5, the difference is considered highly significant. The difference of 5 in AIC corresponds to the difference in likelihood by exp(−2.5). For a Gaussian distribution, this suggests a deviation of $\sqrt{5}\sigma$ from the mean.

Between the top and bottom groups of estimation shown in Fig. 3, ΔAIC is measured as 6.8, and 5.1 between the lower and higher third of ranks for global and Japan catalogues, respectively. For California catalogue, the statistical significance is not guaranteed by ΔAIC.

Data availability. The earthquake catalogue data are available in refs 14–16. All other data that support the findings of this study are available from the corresponding author upon request.